Three-dimensional whispering gallery modes in InGaAs nanoneedle lasers on silicon

Cite as: Appl. Phys. Lett. **105**, 111105 (2014); https://doi.org/10.1063/1.4895920
Submitted: 24 July 2014 . Accepted: 29 August 2014 . Published Online: 16 September 2014

T.-T. D. Tran, R. Chen, K. W. Ng, W. S. Ko, F. Lu, and C. J. Chang-Hasnain

Three-dimensional whispering gallery modes in InGaAs nanoneedle lasers on silicon

T.-T. D. Tran, R. Chen, K. W. Ng, W. S. Ko, F. Lu, and C. J. Chang-Hasnain[a)]
Applied Science and Technology Group and Department of Electrical Engineering and Computer Sciences, University of California, Berkeley, California 94720, USA

(Received 24 July 2014; accepted 29 August 2014; published online 16 September 2014)

As-grown InGaAs nanoneedle lasers, synthesized at complementary metal–oxide–semiconductor compatible temperatures on polycrystalline and crystalline silicon substrates, were studied in photoluminescence experiments. Radiation patterns of three-dimensional whispering gallery modes were observed upon optically pumping the needles above the lasing threshold. Using the radiation patterns as well as finite-difference-time-domain simulations and polarization measurements, all modal numbers of the three-dimensional whispering gallery modes could be identified. © *2014 AIP Publishing LLC*. [http://dx.doi.org/10.1063/1.4895920]

The realization of laser sources on silicon substrates could open a pathway to on-chip communication with large communication bandwidths and low power consumption,[1] but the integration of optical gain materials onto silicon remains difficult due to silicon's indirect bandgap, as well as its differences in lattice constants, thermal expansion coefficients, and polarity with direct-bandgap compound semiconductor materials.[2] Heterogeneous integration of lasers on silicon could be either monolithic in nature,[3–6] or based on wafer bonding.[1,7,8] In bonding approaches, it is possible to manufacture the photonic and electronic chips independently, each with optimized materials choices and processing technologies, before they are bonded together. This could allow bonding approaches to achieve higher yields and a level of maturity sooner.[1] Monolithic integration, on the other hand, could possibly allow for closer integration of photonic and electronic functions, as well as for streamlined manufacturing with lower costs.[9]

Here, we study the lasing modes in single, as-grown $In_{0.22}Ga_{0.78}As$ nanoneedles epitaxially grown on (001)-silicon and polysilicon.[10] Lasers grown on these substrates could have technological relevance since poly-Si is routinely deposited on various low-cost substrates such as glass or silicon-on-insulator (SOI) wafers, while (100)-Si substrates are prevalent in complementary metal–oxide–semiconductor (CMOS) electronics. Furthermore, with a catalyst-free growth at a temperature of 400 °C, nanoneedles could be compatible with back-end integration into standard CMOS technology. Compatibility of the nanoneedle growth with metal-oxide-semiconductor field-effect transistors (MOSFETs) has been previously demonstrated.[11] Fig. 1(a) shows a scanning electron microscope (SEM) image of needles grown near the cleaved edge of an (001)-silicon substrate from side-view.

The key benefit of self-assembled nanowires and nanowire-like structures such as nanoneedles is that their small sizes and non-planar geometry allow for efficient lattice strain relaxation, enabling the growth of high quality III-V materials on silicon.[12–15] Lasing applications are of particular interest for semiconductor nanowires as such structures can provide both, optical gain and waveguiding.[16–18] By reducing the laser volume to the order of cubic of wavelength, power consumption could be significantly reduced in nanowire lasers.[19]

However, III-V nanowires grown on silicon do not exhibit significant index contrast between wire and substrate. So, to realize nanowire lasers, the wires are often being removed from the growth substrate and laid horizontally on a substrate with low refractive index such as SiO_2, so that both end-facets of the nanowires exhibit highly reflective semiconductor/air interfaces, which can then facilitate optical feedback.[20,21] Alternatively, it has also been shown that on-chip external cavities can be fabricated around the nanowires.[6]

If the semiconductor wire diameters are large enough, i.e., similar to the wavelength of the light, then single wire can support helical waveguide modes with high azimuthal modal numbers, which can then form three-dimensional (3D) whispering gallery modes (WGMs) inside the wires.[22,23] 3D-WGMs are commonly found in prolate shaped resonators.[24,25] Even in as-grown, free-standing wires the quality factor of such cavity modes can be high enough to enable lasing; it was previously reported that InGaAs nanoneedles grown on silicon can exhibit single mode lasing at room temperature upon optical pumping.[26] Unlike two-dimensional (2D) WGMs found in flat resonators such as micro disks,[27] 3D-WGMs also exhibit net propagation along

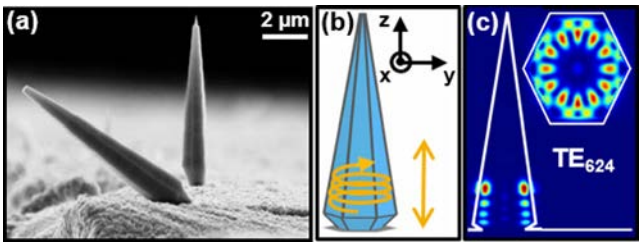

FIG. 1. (a) SEM image of nanoneedles grown on edge of (100) silicon. (b) Schematic of nanoneedle. 3D-WGMs can be thought of rays that propagate helically within the needle. (c) Vertical cross-section of simulated electric intensity profile of TE_{624} mode inside a needle. The inset shows a horizontal cross-sectional view of the mode.

[a)]Electronic mail: cch@berkeley.edu

axial directions: as indicated in Fig. 1(b), the modes can be thought of consisting of rays that propagate back and forth along the needle axis like for Fabry-Perot (FP) modes, while simultaneously revolving around the needle axis as for 2D-WGMs. To identify a cavity mode completely it is necessary to know the polarization as well as the modal numbers m, n, and k, which denote the azimuthal, radial, and axial order, respectively. (The axial order could also be called FP order.) In this paper, we will denote the mode numbers in hexadecimal representation to avoid confusion. The polarization could be either predominantly transverse-electric (TE), i.e., polarized perpendicular to needle axis, or predominantly transverse-magnetic (TM), i.e., polarized parallel to needle axis. (It should be noted that since 3D-WGMs are not purely TE- or TM-polarized it would be more accurate to denote the two possible polarization-states as EH and HE,[28] but to keep the notation consistent with published literature on WGMs in nanowires,[22,23] we will denote the mode polarization as TE or TM.) As an example, Fig. 1(c) shows electric intensity profiles obtained from finite-difference-time-domain (FDTD) simulations of the TE_{624} cavity mode within a nanoneedle. It can be seen that the mode is confined to the base of the needles. This is because at the needle top the diameter is too small to support the TE_{62} waveguide mode.

A very common approach to identify optical modes in very small nano- and microstructures is to match their calculated or simulated resonance wavelengths of modes with experimentally obtained spectra.[22] Such methods are suitable in cases in which the modal spacing is large enough to avoid ambiguities. However, in the cases in which different cavity modes exhibit resonance wavelengths very close to each other, comparing experimentally observed resonance wavelengths with calculations/simulations is often not sufficient. It is also possible to utilize mode profiles to identify modes. To image the mode profiles of small resonators it is possible to use near-field scanning microscopy (NSOM),[29] or cathodoluminescence microscopy.[30] Conventional optical microscopy, on the other hand, is often not suitable to image optical modes in nano- or microresonators as the spatial resolution is too low. However, if the structures are lasing then the emitted radiation will be directional, and it can be possible to use optical microscopy to capture radiation patterns which are distinctive of particular modes.

In this report, radiation patterns of lasing as-grown nanoneedles were experimentally studied and combined with information obtained from FDTD simulations and polarization measurements the lasing modes could be identified. The nanoneedle growth was carried out in an Emcore D75 Metal-Organic-Chemical-Vapor-Deposition (MOCVD) reactor at a temperature of 400 °C without the introduction of catalysts.[31,32] The nanoneedles studied here consist of a bulk $In_{0.20}Ga_{0.80}As$ core capped with a 120 nm thick layer of GaAs for surface passivation, and had diameters between 0.85 μm and 1.5 μm, depending on the growth time. The aspect ratio (height to base diameter) of the needles is about 6. The needles were grown on poly-Si and (001)-Si substrates. Since the needle growth direction follows the $\langle 111 \rangle$ crystal directions of the substrate,[31,32] they grew in slanted directions with respect to the substrate surface. The slanted growth directions allow for studying the needles from side-view when looking at the substrate surface from the top. The tapered hexagonal shape can be seen from the SEM in Fig. 1(a), and is also schematically shown in Fig. 1(b). Transmission electron microscopy studies (TEM) revealed that the material crystal structure is wurtzite, whereby the crystal c-axis is oriented parallel to the long axis of the needle.[32] The core-shell growth mode of the needles enables extending the needle base diameter to micrometer-dimensions while maintaining a single-crystal quality. TEM studies also showed that near the InGaAs/Silicon interface the pillars often exhibit stacking disorders.[32] But since the stacking faults terminate horizontally at the needle sidewalls they do not propagate to the main body of the needle, which remains free of misfit dislocations.[32]

In our photoluminescence experiments, the needles were studied from side-view. The needles were optically pumped by a 765 nm femtosecond laser (120 fs pulse duration, 80 MHz repetition rate, 2.4 μm spot size on sample) at liquid helium temperatures near 4 K. The needle emission was collected by an objective with a numerical aperture of 0.7, and subsequently either imaged with a charge-coupled device (CCD) camera or analysed in a spectrometer. In Figs. 2(a)–2(i) experimental and simulated data obtained from an as-grown single needle laser with a base diameter of 1.2 μm and a length of 7 μm is shown. Fig. 2(a) exhibits the light-light characteristic of the laser, showing that the lasing threshold is at about $P_{th} = 1.6$ mW pump power, as indicated by the kink in the curve. Fig. 2(b) shows the laser spectra for polarizations parallel and perpendicular to the needle. A polarization ratio (TE versus TM) of 16 dB, and a side mode suppression ratio (SMSR) of 17 dB could be seen. The fact that the needles' laser emission is TE-polarized might be surprising as TM-polarized WGMs usually exhibit higher Q-factors,[33] and we ascribe this finding to an anisotropic optical matrix element of the wurtzite material which is stronger perpendicular to the c-axis.[34] Indeed, as seen in Fig. 2(b) the spontaneous emission from the needle is 3 times more polarized perpendicular to the needle. Fig. 2(d) shows the radiation pattern of the lasing mode at a pump power of $1.5P_{th}$. The orientation of the needle in that measurement can be inferred by comparing the coordinate system shown in Fig. 2(d) with the coordinate system shown in Fig. 1(b). The radiation pattern reveals 4 lobes along a line perpendicular to the long axis of the needle. Since only one set of lobes is visible in the direction of the needle's long axis, it can be inferred that the axial order of the lasing mode is $k = 1$. To identify the nature of the lasing mode, optical 3D-FDTD simulations have been performed in which several TE-polarized resonator modes with $k = 1$ were found: TE_{A11} (850 nm), TE_{911} (925 nm), TE_{811} (1010 nm), and TE_{621} (926 nm). (The numbers in parentheses denote the resonance wavelengths.) As an example, the simulated cavity spectrum of TE_{62k} modes is shown in Fig. 2(c). Since the needle lases at 935 nm, the TE_{911} and TE_{631} modes are most consistent with the simulations. Figs. 2(e) and 2(f) and Figs. 2(g) and 2(h) show cross sections of the electric-field intensity of the TE_{621} and TE_{911} modes. It can be seen that a TE_{911} mode should exhibit 2 lobes when looking at the needle from x-direction, whereas for the TE_{631} mode, 4 lobes would be expected. Thus, it can be concluded that TE_{631} is the likely

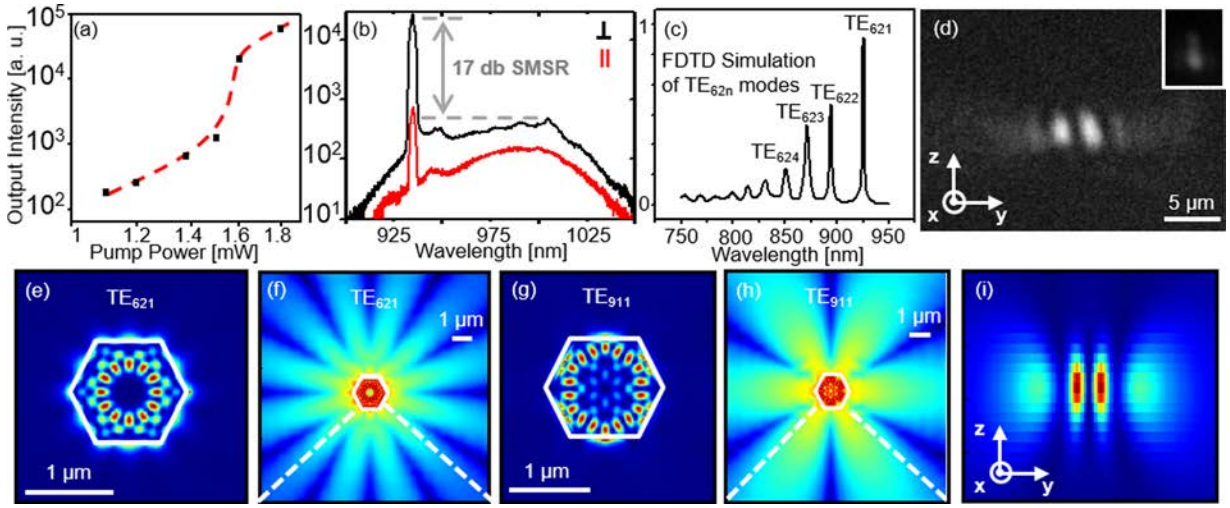

FIG. 2. (a) Light-light characteristic of nanoneedle laser. The kink in the curve shows that the lasing threshold is at $P_{th} = 1.6$ mW pump power. (b) TE ($\perp$) and TM ($||$) polarization of lasing spectrum at 1.8 mW pump power (1.1 P_{th}). (c) Simulated cavity spectrum of TE_{62k} modes in studied needle. (d) Observed radiation pattern for pump powers above the lasing threshold. The orientation of the needle in the image can be inferred by comparing the indicated coordinate system with the coordinate system shown in Fig. 1(b). The inset shows the needle emission for a pump power of 0.5 P_{th}. (e)–(h) Horizontal cross sections of simulated electric intensity profile of TE_{621} mode (in (e) and (f)) and TE_{911} mode (in (g) and (h)) shown in linear false color scale (for (e) and (g)), and logarithmic false color scale (for (f) and (h)). In (f) and (h), the collection cone of the objective used in this experiment is indicated by dotted lines. (i) Simulated radiation pattern of TE_{621} mode as seen from side-view (x-direction).

lasing mode. Fig. 2(i) shows how the TE_{621} mode is supposed to look like when looking at the needle from side-view (x-direction); the simulated pattern in Fig. 2(i) and the experimentally observed pattern in Fig. 2(d) match well. In addition, the quality factors for the TE_{621} (TE_{911}) mode have been simulated to be 360 (240), which is another indication that the lasing mode is the TE_{621} mode.

Modes with $k > 1$ have also been observed. Figs. 3(a)–3(g) show experimental data obtained from of a needle with a diameter of 860 nm and a length of 8 μm. The light-light curve for this needle can be seen in Fig. 3(a), showing that the lasing threshold is at about $P_{th} = 1.8$ mW pump power. From Fig. 3(b), it can be seen the lasing emission is strongly TE polarized, with a polarization ratio larger than 11 dB. The SMSR at a pump power of $1.9P_{th}$ is 15 dB. Figs. 3(c)–3(f) show radiation patterns at different pump power levels. It can be seen that the mode pattern becomes visible for pump powers higher than the lasing threshold of 1.8 mW. The polarization dependence of the pattern (see Fig. 3(g)) provides further evidence that the radiation pattern stems from the lasing mode. The radiation pattern seen in Fig. 3(f) exhibits 2 lobes in axial direction, which shows that $k = 2$.

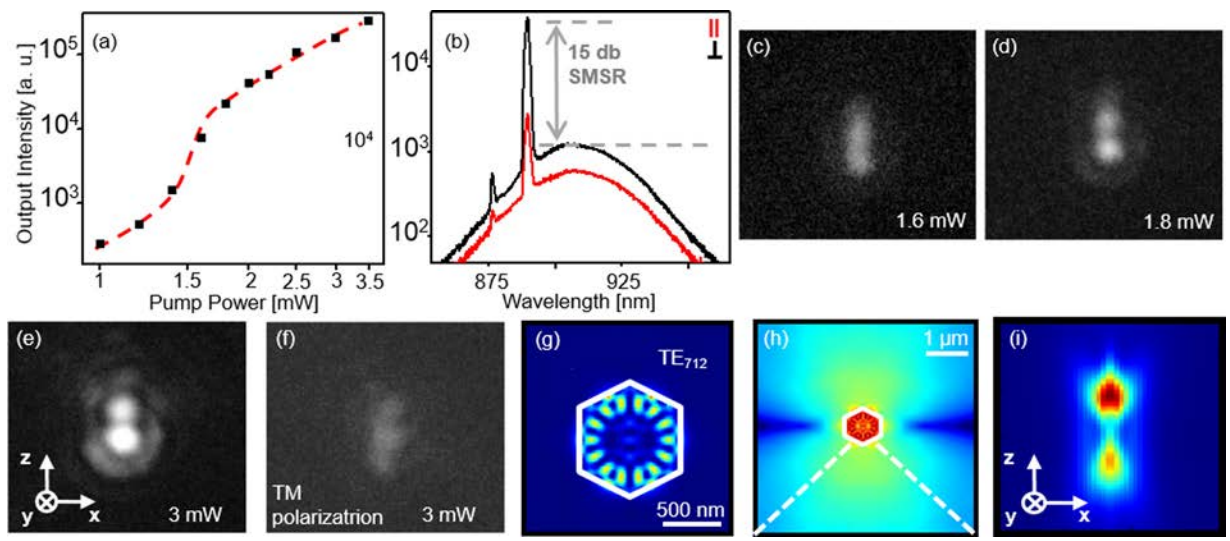

FIG. 3. (a) Light-Light characteristic of nanoneedle laser. The kink in the curve shows that the lasing threshold is at $P_{th} = 1.8$ mW pump power. (b) TE ($\perp$) and TM ($||$) polarization of lasing spectrum at pump power of 1.7 P_{th}. (c)–(f) Observed radiation patterns of needle under different pump power levels: (c) below threshold ~0.9 P_{th}, (d) ~threshold, and (e) 1.7 P_{th}. It can be seen that the lasing mode becomes visible for pump powers of P_{th} and higher. The coordinate system used in images (c)–(f) is labelled in (e), which is consistent with the coordinate system shown in Fig. 1(b). (f) TM-polarized component of radiation pattern at pump power of 1.7 P_{th}. The absence of the distinctive radiation pattern shows that the mode is strongly TE-polarized. (g)–(i) Horizontal cross section of simulated electric intensity profile of TE_{712} mode shown in linear false color scale (for (g)), and logarithmic false color scale (for (h)). In (h), the collection cone of the objective used in this experiment is indicated by dotted lines. (i) Simulated radiation pattern of TE_{712} mode as seen from side-view (-y-direction). This is in good agreement with Figs. 3(d) and 3(e).

FDTD simulations were used to identify possible TE polarized modes with k = 2: TE_{812} (782 nm), TE_{712} (872 nm), and TE_{612} (966 nm). (The resonance wavelengths of the modes are denoted in parentheses.) Since the needle lases at a wavelength of 890 nm, the TE_{712} mode is the likely lasing mode. FDTD simulations of the TE_{712} mode (see Figs. 3(g)–3(i)) confirm that the observed radiation pattern could stem from this mode. In the spectrum shown in Fig. 3(b), a small second peak can be seen at a wavelength of 875 nm. This peak could be attributed to the TE_{713} mode which, in FDTD simulations, exhibits a resonance wavelength that is 20 nm to the blue side of the TE_{712} mode.

In summary, by studying slanted nanoneedles near field patterns of the lasing modes could be measured from side-view. The lasing modes, including all 3 quantum numbers, could be identified with optical microscopy by comparisons of radiation patterns, polarization data, and FDTD simulation results.

The authors acknowledge the support of United States Department of Defense National Security Science and Engineering Faculty Fellowship N00244-09-1-0013 and N00244-09-1-0080, and the Center for Energy Efficient Electronics Science (National Science Foundation (NSF) award ECCS-0939514). Furthermore, the authors acknowledge support through the NSF Center for Integrated Access Networks (EEC-08120702) and NSF award 1335609.

[1]M. Ashghari and A. Krishnamoorthy, Nat. Photonics **5**, 268 (2011).
[2]S. F. Fang, K. Adomi, S. Iyer, H. Morkoc, H. Zabel, C. Choi, and N. Otsuka, J. Appl. Phys. **68**, R31 (1990).
[3]M. Groenert, C. W. Leitz, A. J. Pitera, V. Yang, H. Lee, R. J. Ram, and E. A. Fitzgerald, J. Appl. Phys. **93**, 362 (2003).
[4]R. E. Cammacho-Aguilera, Y. Cai, N. Patel, J. T. Bessette, M. Romagnoli, L. C. Kimerling, and J. Michel, Opt. Express **20**, 11316 (2012).
[5]S. Liebich, M. Zimprich, A. beyer, C. Lange, D. J. Franzbach, S. Chatterjee, N. Hossain, S. J. Sweeney, K. Volz, B. Kunert, and W. Stolz, Appl. Phys. Lett. **99**, 071109 (2011).
[6]T. Frost, S. Jahangir, E. Stark, S. Deshpande, A. Hazari, C. Zhao, B. S. Ooi, and P. Bhattacharya, Nano Lett. **14**, 4535 (2014).
[7]H. Park, A. Fang, S. Kodama, and J. Bowers, Opt. Express **13**(23), 9460–9464 (2005).
[8]H. Yang, D. Zhao, S. Chuwongin, J. H. Seo, W. Yang, Y. Shuai, J. Berggren, M. Hammar, Z. Ma, and W. Zhou, Nat. Photonics **6**, 615–620 (2012).
[9]E. Fuchs, E. Kirchain, and S. Liu, J. Lightwave Technol. **29**, 2319 (2011).
[10]K. W. Ng, T.-T. D. Tran, W. S. Ko, R. Chen, F. Lu, and C. J. Chang-Hasnain, Nano Lett. **13**, 5931–5937 (2013).
[11]F. Lu, T.-T. D. Tran, W. S. Ko, K. W. Ng, R. Chen, and C. Chang-Hasnain, Opt. Express **20**, 12171 (2012).
[12]T. Mårtensson, C. P. T. Svensson, B. A. Wacaser, M. W. Larsson, W. Seifert, K. Deppert, A. Gustafsson, L. R. Wallenberg, and L. Samuelson, Nano Lett. **4**, 1987 (2004).
[13]L. C. Chuang, M. Moewe, C. Chase, N. P. Kobayashi, C. J. Chang-Hasnain, and S. Crankshaw, Appl. Phys Lett. **90**, 043115 (2007).
[14]K. Tomioka, J. Motohisa, S. Hara, and T. Fukui, Nano Lett. **8**, 3475 (2008).
[15]W. Wei, X. Y. Bao, C. Soci, Y. Ding, Z. L. Wang, and D. Wang, Nano Lett. **9**, 2926 (2009).
[16]M. H. Huang, S. Mao, H. Feick, H. Yan, Y. Wu, H. Kind, E. Weber, R. Russo, and P. Yang, Science **292**, 1897 (2001).
[17]X. Duan, Y. Huang, R. Argarwal, and C. M. Lieber, Nature **421**, 241 (2003).
[18]A. V. Maslov and C. Z. Ning, Opt. Lett. **29**, 572 (2004).
[19]M. T. Hill, Y. S. Oei, B. Smalbrugge, Y. C. Zhu, T. de Vries, P. J. van Veldhoven, F. W. M. van Otten, T. J. Erjkemns, J. P. Turkiewicz, H. de Waardt, E. J. Geluk, S. H. Kwon, Y. H. Lee, R. Nötzel, and M. K. Smit, Nat. Photonics **1**, 589 (2007).
[20]B. Mayer, D. Rudolph, J. Schnell, S. Morkötter, J. Winnerl, J. Treu, K. Müller, G. Bracher, G. Abstreiter, G. Koblmüller, and J. J. Finley, Nat. Commun. **4**, 2931 (2013).
[21]D. Saxena, S. Mokkapati, P. Parkinson, N. Jiang, Q. Gao, H. H. Tan, and C. Jagadish, Nat. Photonics. **7**, 963 (2013).
[22]C. Czekalla, C. Sturm, R. Schmidt-Grund, B. Cao, M. Lorenz, and M. Grundmann, Appl. Phys. Lett. **92**, 241102 (2008).
[23]G. Pavlovic, G. Malpuech, and N. A. Gippius, Phys. Rev. B **82**, 195328 (2010).
[24]M. Sumetsky, Opt. Lett. **29**, 8 (2004).
[25]P. Bianucci, X. Wang, J. G. C. Veinot, and A. Meldrum, Opt. Express **18**, 8466 (2010).
[26]R. Chen, T. T. D. Tran, K. W. Ng, W. S. Ko, L. C. Chuang, F. G. Sedwick, and C. J. Chang-Hasnain, Nat. Photonics **5**, 170 (2011).
[27]S. L. McCall, A. F. J. Levi, R. E. Slusher, S. J. Pearton, and R. A. Logan, Appl. Phys. Lett. **60**, 289 (1992).
[28]D. Marcuse, *Light Transmission Optics* (Van Nostrand Reinhold, New York, 1972).
[29]S. Götzinger, S. Demmerer, O. Benson, and V. Sandogdar, J. Microsc. **202**, 117 (2001).
[30]N. W. Wang, Y. H. Yang, and G. W. Yang, Appl. Phys. Let. **97**, 041917 (2010).
[31]M. Moewe, L. C. Chuang, S. Crankshaw, C. Chase, and C. J. Chang-Hasnain, Appl. Phys. Lett. **93**, 023116 (2008).
[32]K. W. Ng, W. S. Ko, T. T. D. Tran, R. Chen, M. V. Nazarenko, F. Lu, V. G. Dubrovskii, M. Kamp, A. Forchel, and C. J. Chang-Hasnain, ACS Nano **7**, 100 (2013).
[33]C. G. B. Garret, W. Kaiser, and W. L. Bond, Phys. Rev. **124**, 1807 (1961).
[34]D. Spirkoska, A. L. Efros, W. R. L. Lambrecht, T. Cheiwchanchamangij, A. Fontcuberta i Morral, and G. Abstreiter, Phys. Rev B **85**, 045309 (2012).